united nations
educational, scientific
and cultural
organization

international atomic
energy agency

the
abdus salam
international centre for theoretical physics

SMR: 1133/11

WINTER COLLEGE ON
SPECTROSCOPY AND APPLICATIONS

(8 - 26 February 1999)

"Laser Spectroscopy of Atoms"

presented by:

Aslam BAIG
Universität Heidelberg
Physikalisch-Chemisches Institut
Im Neuenheimer Feld 253
D-69120 Heidelberg
Germany

Laser Spectroscopy of Atoms

M. Aslam Baig
Atomic and Molecular Physics Laboratory, Department of Physics,
Quaid-i-Azam University, Islamabad, Pakistan

Abstract

Applications of dye lasers for the studies of atomic structure using thermionic diode and atomic beam apparatus are presented. Multi-photon and multi-step excitation schemes are exploited to investigate the high Rydberg levels of the alkalis, alkaline earths elements and inert gases. A few examples of the interesting spectra are discussed and the interpretation is supplemented by the Multi Channel quantum defect theory.

Introduction:

Multi-step and multi-photon excitation spectroscopy has played a vital role to probe the excited states of atoms and molecules as it provides detailed information about the nature of the bound states of atoms, and the information gathered are complementary to the standard photo absorption spectra. This technique has been used to measure the positions of the atomic energy levels and the atomic fine structure studies. The main advantage of the multiphoton excitation is the observation of the excited states possessing higher angular momenta that are not accessible by the single photon excitation from the ground state. For example, the one photon absorption spectra of inert gases reveal $p^5(^2P_{1/2,3/2})$ ns and nd J = 1 odd parity excited Rydberg levels and the two photon excitation yield $p^5(^2P_{1/2,3/2})$ np and nf J = 0 and 2 even parity levels. However, using the three-photon excitation, the $p^5(^2P_{1/2,3/2})$ ns, nd and ng odd parity J = 1 and 3 series can be approached whereas, with four photon excitation the accessible even parity channels become $p^5(^2P_{1/2,3/2})$ np, nf and nh with J = 0, 2 and 4. In the following section, a few of examples of multi-step and multi-photon excitation in atoms are presented.

1. Two-Photon and Two-step Excitation

The photoionization cross section of strontium is dominated by a strong autoionizing level at about $\approx$ 470 cm^{-1} above the first ionization threshold. This level can be excited either

from the ground level via two-photon excitation at 431nm or by the two-step excitation with two different dye lasers where the first laser is fixed on the resonance transition to the 5s5p $^1P_1$ level (λ_1 = 460 nm) while the second laser is tuned over the autoionizing resonance around λ_2 = 405 nm. This autoionizing level was assigned as $4d^2\ ^1D_2$. Based on the eigen channel and R-Matrix calculations, Aymar et al (1984) assigned this level as a mixture of $4d^2$ and $5p^2$ configurations, where the $5p^2$ configuration is predominant. The absolute photoionizaion cross-section for transition from 5s5p $^1P_1$ to $(4d^2 + 5p^2)\ ^1D_2$ has been recently measured using a thermionic diode ion detector and its peak cross section was reported as 5600 Mb ($5.6x10^{-15}$ cm^2) with 20% uncertainty. The Fano formula (Fano 1961) for an isolated autoionization resonance was fitted to the measured points to extract the line shape q-parameter, the width of the profile and the resonance energy.

This autoionizing level has been excited via two different paths i.e. two-photon excitation with a single laser and two-step excitation with two different lasers where the intermediate level was the 5s5p $^1P_1$ resonance level. By using an atomic beam apparatus the collisional contributions were minimized. Figure 1 shows the line profile of the autoionizing resonance resulting from the two-photon excitation covering the laser photon energy from 22900 cm^{-1} to 23300 cm^{-1}. The arrow at 22966 cm^{-1} shows the first ionization threshold.

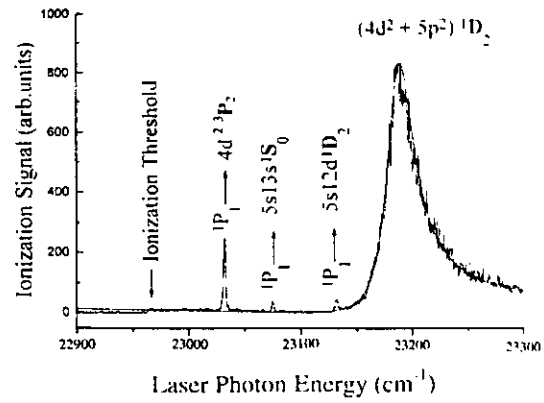

Fig.1: *Two photon excitation spectra of strontium showing the $(4d^2+5p^2)^1D_2$ autoionizing resonance.*

There are evidently three extra resonances between the ionization threshold and the strong autoionizing resonance. The resonances observed at $\hbar\omega$ = 23031 cm^{-1}, $\hbar\omega$ = 23075 cm^{-1} and $\hbar\omega$ = 23162 cm^{-1} are not associated with any intermediate multiphoton resonances from the ground state of strontium. The origin of their appearance becomes clear from the Fig. 2. These levels correspond to transitions between the excited 5s5p $^1P_1$ level and the $4d^2\,^3P_2$, 5s13s $^1S_0$ and 5s12d $^1D_2$ levels respectively. Energetically these level lie below the first ionization threshold but here appear as displaced resonances. Their term energies, (photon energy + energy of 5s5p $^1P_1$ level) turn out to be 44729.6 cm^{-1}, 44793.4 cm^{-1} and 44829.7 cm^{-1}. The appearance of these lines indicates that the 5s5p $^1P_1$ level is considerably populated.

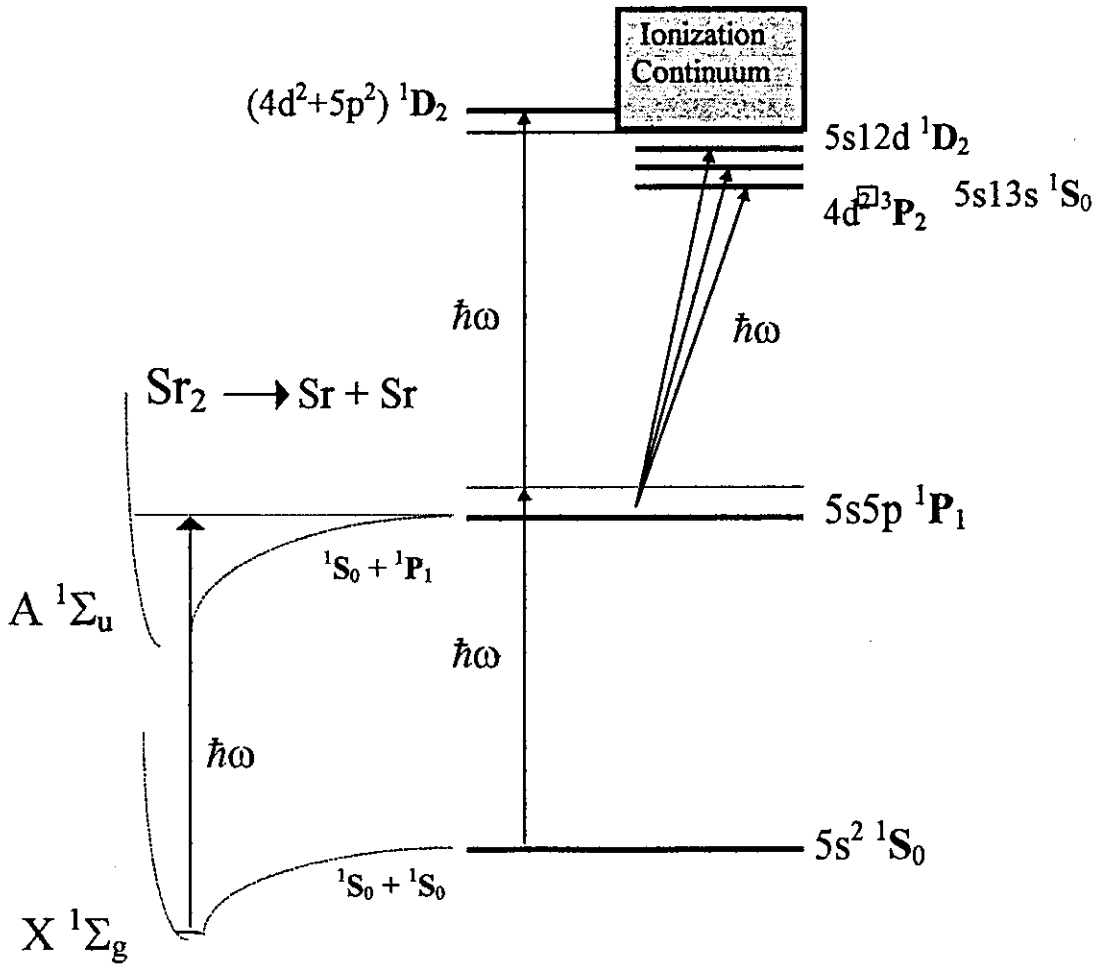

Fig.2 *The energy level diagram of the strontium atom and the strontium molecule showing the sequential excitation of the $4d^2\,^3P_2$,, 5s13s $^1S_0$ and 5s12d $^1D_2$ levels from the 5s5p $^1P_1$ level as a result of molecular dissociation.*

These resonances appear only in the two-photon excitation experiment when the laser is scanned from 22900 to 23300 cm^{-1}. The nearest real level to the virtual level that can play a significant role is 5s5p $^1P_1$ at 21698.482 cm^{-1}. Therefore, the detuning from the nearest real level is about 1200 cm^{-1}. The possible mechanism of 5s5p $^1P_1$ population is the dissociation of strontium molecules which are always present in the atomic vapor. The X $^1\Sigma_g$ ground state of strontium molecule arises from the two ground state strontium atoms. This molecular state is very weakly bound with dissociation energy of about 1088 cm^{-1}. The Sr_2 molecule absorbs a photon and is excited to the dissociation continuum of the $A^1\Sigma_u$ state which leads to the dissociation into two strontium atoms, one in the ground state Sr ($5s^2\ ^1S_0$) and the other in the first excited state Sr*($5s5p\ ^1P_1$).

$$Sr_2\, X\, ^1\Sigma_g \rightarrow (Sr_2)^* \rightarrow Sr(5s5p\ ^1P_1) + Sr(5s^2\ ^1S_0)$$

Since the dissociation process is very fast ($\approx 10^{-12}$s), it is possible that the atoms in the 5s5p $^1P_1$ excited state absorb a second photon from the same laser pulse ($\approx 6.10^{-9}$s) which leads to the excitation of the observed resonances, 5s5p $^1P_1 \rightarrow 4d^2\ ^3P_2$, 13s $^1S_0$ and 12d $^1D_2$. The atoms in these excited states then become ionized either by absorbing another photon from the same laser pulse or due to the black body radiation. The process is termed as sequential excitation and similar excitations have been observed in alkali atoms.

Figure 3 shows the line profile of the ($4d^2 + 5p^2$) $^1D_2$ level resulting from the two-color two-step excitation covering the same total energy as in figure 1. Our interest is to investigate the difference in the line shapes of an autoionizing resonance by the non-resonant two-photon excitation and by the resonant two-step excitation processes. The line shape parameters have been extracted by fitting the observed profiles of the autoionizing resonance using the two channel quantum defect theory (MQDT). In the two channel model the photoionization cross section is represented by the expression:

$$\sigma = KD_1^2 \left\{ \frac{\left(\frac{1}{R_{12}^2} \tan^2 \pi(\nu_2 + \delta_2) - \frac{D_2}{D_1 R_{12}} \right)^2}{\frac{1}{R_{12}^4} \tan^2 \pi(\nu_2 + \delta_2) + 1} \right\} \qquad (1)$$

By comparing it with the Fano's formulation,

$$\sigma = KD_1^2 \frac{(\varepsilon + q)^2}{\varepsilon^2 + 1} \text{ , where } \varepsilon = \frac{2(E - E_r)}{\Gamma} \qquad (2)$$

these parameters can be represented by the following relations:

$$\varepsilon = \tan \pi(\nu_2 + \delta_2) / R_{12}^2 \qquad (3)$$

$$\Gamma = \frac{4R_y R_{12}^2}{\pi \nu_2^3} \quad (cm^{-1}); \quad \text{and} \quad q = -\frac{D_2}{R_{12} D_1} \qquad (4)$$

Here ν_2 is the effective quantum number with respect to the second ionization threshold, R_y is the Rydberg constant, R_{12} is the measure of the interaction between the continuum and the closed channel while D_1 and D_2 are proportional to the transition moments.

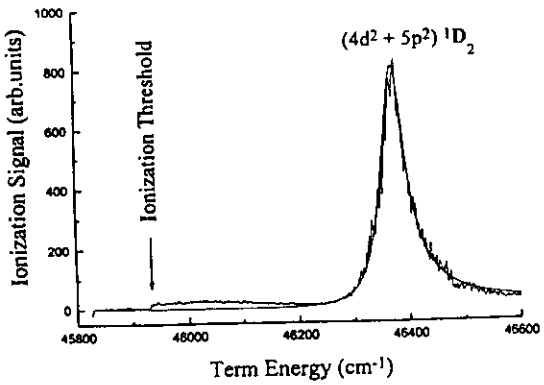

Fig. 3. *Two-step excitation spectra of strontium showing the* $(4d^2 + 5p^2)^1D_2$ *autoionizing resonance.*

Fitting the expression (1) for the photoionization cross-section to the observed data is straightforward for the two-step excitation process. Whereas, for the two-photon excitation case, D_1 and D_2 are not constants but are proportional to the photon field. However, since the ratio D_2/D_1 is field independent, the line shape factor, enclosed in the brackets, is also field independent. The cross-section, although increases linearly with the photon intensity through D_1^2, its line shape nevertheless remains the same. Therefore, we may fit the two- photon case with the same expression as used in the two-step case. However, D_1 will have different meaning in both the cases. In the two-step excitation it represents the transition moment between the 5s5p $^1P_1$ level and the continuum whereas, in the case of two-photon excitation it represents the transition moment between the $5s^2$ $^1S_0$ ground state and the ionization continuum. The full curve in the figures is the calculated line profiles using expression (1) that are overlapped with the experimental profiles. The nearly perfect match of the experimental and the simulated profiles is rather surprising. The following MQDT parameters have been determined:

Excitation Path	R_{12}	δ_2	D_1	D_2
Two-photon excitation	0.095	0.212	-5.00	2.73
Two-step excitation	0.092	0.212	-2.55	2.73

Interestingly, three parameters, R_{12}, δ_2 and D_2, remain nearly the same except the D_1 in the fitted profiles measured by the two different excitation pathways. Even more interesting is that D_1 is almost twice in the two-photon excitation as compared to the two-step excitation. The profile width Γ depends only on R_{12} and δ_2 that are identical in both the cases. From the values of the parameters the extracted value of FWHM is $\Gamma = 56 \pm 1$ cm^{-1}. It confirms that whatever the excitation path is used to approach an excited level, the width of the autoionizing level remains unaltered. The lineshape 'q' parameter depends on the D_2/D_1 ratio. Its value in the stepwise excitation case turns out to be 10 whereas in the case of two-photon excitation it is 5.7. It is worth mentioning that the ratio of the

absorption cross section at the ionization threshold and that of at the $(4d^2 + 5p^2)\ ^1D_2$ level is in good agreement with the literature reported value.

2. Three Photon Excitation in strontium:

The three-photon excitation spectrum of strontium obtained from the atomic beam set up using the linearly polarized laser photons of energy from 15200 cm^{-1} to 15350 cm^{-1} is shown in Fig.4. There is a clear evidence of two Rydberg series converging to a limit around 15310.7 cm^{-1} that corresponds to the three-photon ionization threshold. The higher members of the series are obscured by a strong resonance adjacent to the three-photon ionization threshold. This strong and broad feature around 15300 cm^{-1} is explained as two-photon resonant three-photon ionization signal through the 5s6s $^1S_0$ level of strontium.

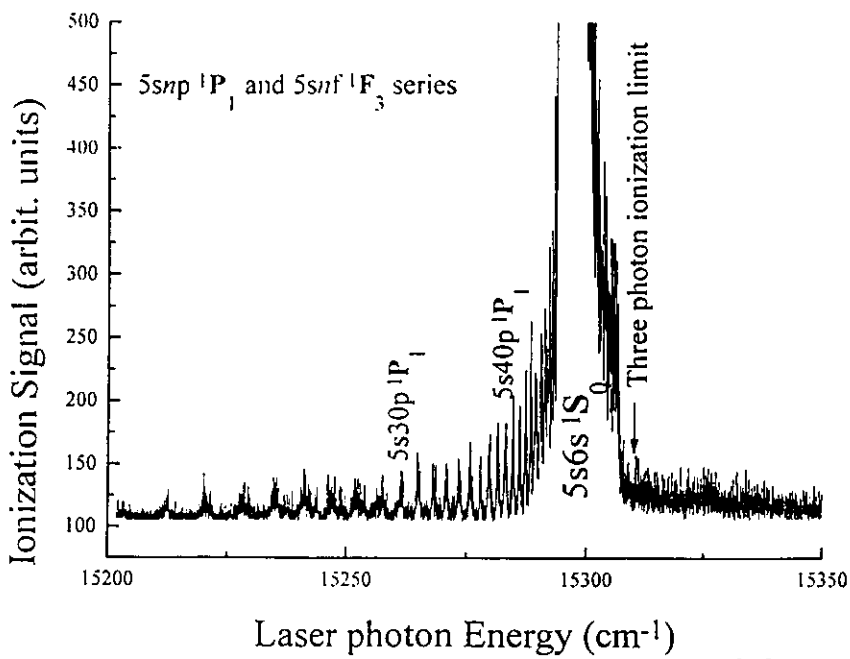

Fig.4 *Data from the atomic beam setup for the laser photon energies from 15200 to 15350 cm-1 showing the three-photon excitation of 5snp 1P1 and 5snf 1F3 series of strontium.*

Fig 5 shows the spectrum obtained from the thermionic diode detector setup. Here again the three photon excitation spectra is apparent along with strong feature corresponding to the 5s6s $^1S_0$ level. However, here in addition a series of energy level markers with successively reducing intensity are observed on the lower energy side of the spectrum, which were missing in the spectra obtained from the atomic beam setup. These markers correspond to the 5s*n*p $^1P_1$ Rydberg levels populated by the sequential excitation from the 5s6s $^1S_0$ level. This kind of excitation is routinely observed in the experiments based on the thermionic diode detector where a reasonable number of dimer are present which are dissociated by the laser photons yielding one atom in the excited level and other in the ground level.

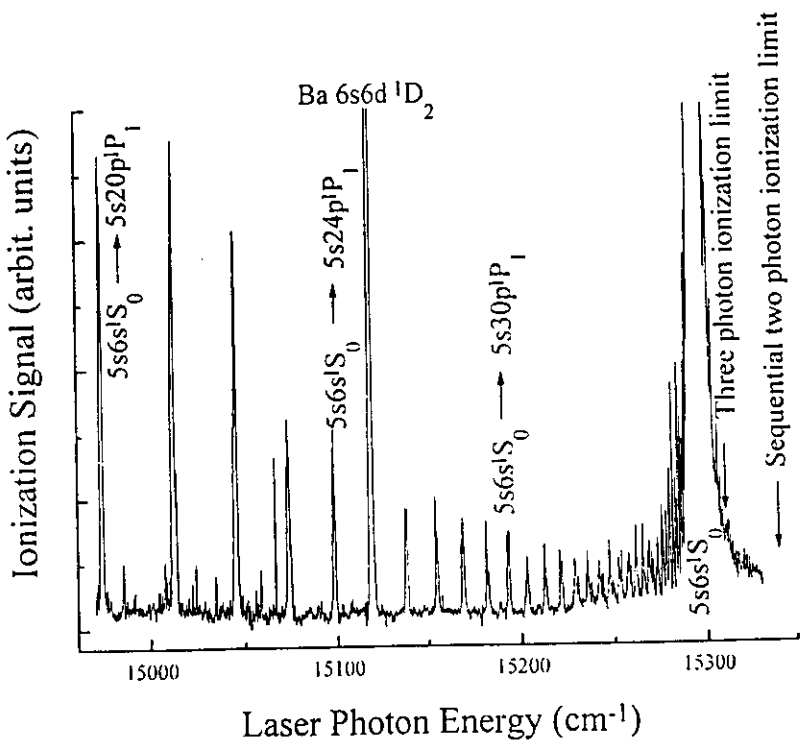

Fig.5. *Data from the thermionic diode setup for the laser photon energies from 14950 to 15350 cm^{-1}. The lower energy region shows the sequential excitation of the 5s*n*p $^1P_1$ series of strontium from the 5s6s $^1S_0$ level. The strong feature at 15118 cm^{-1} is due to 6s5d $^1D_2$ level of barium which is present as impurity.*

The term values of the sequentially excited levels were obtained by adding the energy 30591.8 cm^{-1} of the 5s6s $^1S_0$ level to the laser photon energy whereas, for the three photon excitation these are simply three times the laser photon energy. Since the energies of the 5s*n*p $^1P_1$ Rydberg levels have already been reported with high precision by many groups, therefore there is no need to repeat the tabulation here.

In the region of the intensity minimum around 15240 cm^{-1} the signal due to the sequential excitation 5s*n*p $^1P_1$ is decreasing whereas the signal due to the three-photon excitation is enhancing and finally overlap with the strong two-photon resonant three-photon ionization signal with a peak at 15300 cm^{-1}. The series limits corresponding to the sequential excitation and three-photon excitation lie at 15340.3 cm^{-1} and 15310.7 cm^{-1} respectively and are marked with arrows in the figure. Two very strong lines have also been observed at 15118 cm^{-1} and 15375 cm^{-1} which are identified as barium two photon excited levels 6s6d $^1D_2$ and 6s6d $^3D_2$ respectively, since barium is mostly present as an impurity in the strontium sample. The 6s6d $^1D_2$ level of barium overlap in energy with the 5s25p $^1P_1$ level of strontium that also serves as an energy marker in the present experiment.

In order to assign the observed Rydberg series excited by the three photon process, it is important to look into the selection rules in the electric dipole approximation for three photon transitions from the $5s^2$ $^1S_0$ ground state to the Rydberg series converging to the 5s $^2S_{1/2}$ limit. The strongest selection rules are those of parity and total angular momentum. From the parity selection rule, since the ground state parity is even, the orbital angular momentum of the Rydberg electron must be odd. For the three-photon transitions from the $5s^2$ $^1S_0$ ground state using linearly polarized light, the final state orbital angular momentum has to be p or f. From the total angular momentum selection rules, the total angular momentum of the final state can be 1 or 3. Therefore, the allowed Rydberg series can be described in the LS coupling as 5s*n*p $^1P_1$ and 5s*n*f $^1F_3$. It is worth noting that the higher members are obscured by the 5s6s $^1S_0$ level. For the lower members of the Rydberg series there are two lines that correspond to members of the 5s*n*p $^1P_1$ ($25 \leq n \leq 43$) and 5s*n*f $^1F_3$ ($22 \leq n \leq 26$) series. This is confirmed by comparing their quantum defects with the literature values. It is noted that the spectra obtained from direct three-photon

excitation without an intermediate level, the 5s*n*p $^1P_1$ resonances are stronger than the 5s*n*f $^1F_3$ resonances. It is the first observation of the members of the 5s*n*p $^1P_1$ and 5s*n*f $^1F_3$ series via three-photon excitation in strontium from the ground state.

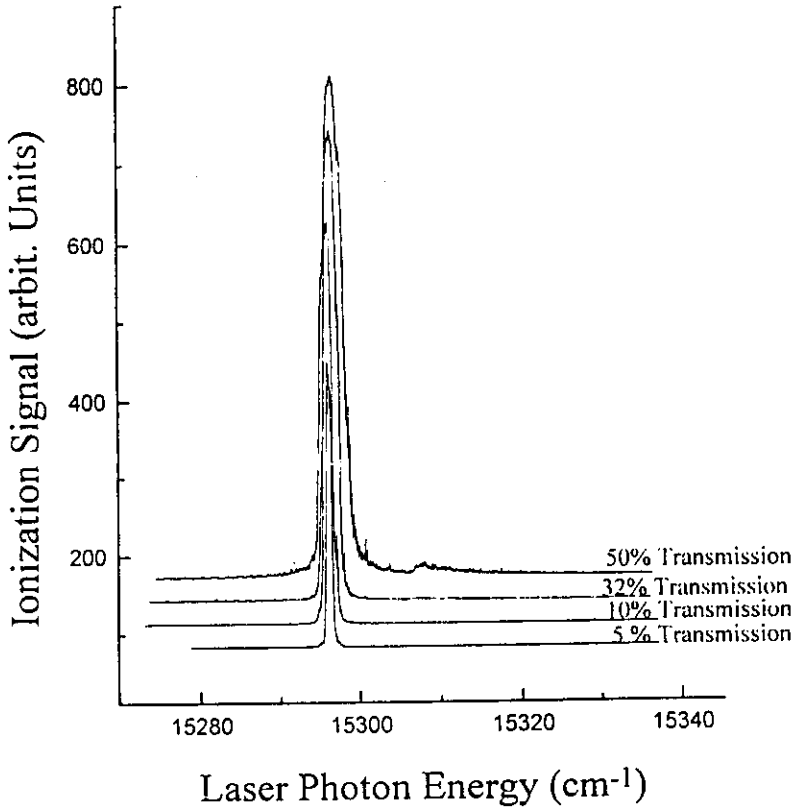

Fig. 6. *Variation of the ionization signal as a function of laser wavelength for various laser intensities.*

Considering the excitation of the 5s*n*p $^1P_1$ Rydberg levels by the atomic beam experiment, the three-photon excitation process, the lowest level observed lies about 235 cm^{-1} below the first ionization threshold. Even this is a high lying Rydberg level and it is well known that the photoionization cross-section for such levels is extremely small. Besides, photoionization cross-section decreases with the photon energy as ω^{-3} but what is observed is an increase in the signal intensity with the laser photon energy. Therefore, the ionization process is not predominantly the photoionization. Instead, it is either ionization due to the blackbody radiation (Cooke and Gallagher 1978) or due to the collisions with

the other atoms, since in both the cases the signal increases with principal quantum number *n*.

In order to investigate the dependence of the line shape and the ionization signal on the laser intensity, neutral density filters of varying strengths were inserted in the dye laser beam. The width of the ionization signal decreases with the increase of the attenuation by the neutral density filters as shown in figure 6. The widths are 3.6 ± 0.4 cm^{-1}, 1.6 ± 0.4 cm^{-1}, 1.0 ± 0.4 cm^{-1} and 0.8 ± 0.4 cm^{-1} for 50%, 32%, 10% and 5% transmissions respectively. A plot of the ionization signal against the laser intensity shows a slop of 3 which confirms that it is a three photon ionization process.

3. Multi-step Excitation in argon

The ground state of argon is $3p^6\ ^1S_0$ and due to the excitation of one of the 3p-subshell electrons to the next available 4s orbital it yields four levels build on the $3p^54s$ configuration, namely $3p^54s[1/2]_{0,1}$ and $3p^54s[3/2]_{1,2}$. The $3p^54s[1/2]_0$ and $3p^54s[3/2]_2$ levels being the metastable levels provide an opportunity to access the high lying Rydberg levels via direct two photon excitation or through the two-step excitation. In principal, a single photon excitation from this level will also be a possibility but it needs a short wavelength 200 nm laser. The life times of the $3p^54s[1/2]_0$ and $3p^54s[3/2]_2$, levels are 44.9 s and 55.9 s respectively (Radzig and Smirnov 1985). It shows that only the $3p^54s[3/2]_2$ level is more promising for the optogalvanic spectroscopic studies. By employing the single photon excitation from the $3p^54s[1/2]_0$ level it is possible to record all the levels possessing the even parity with J = 1 and from the $3p^54s[3/2]_2$ level, the upper levels with J = 1, 2 and 3 are possible. A two-photon excitation from the $3p^54s[3/2]_2$ level will yields all the exited levels with J ranging from 1 to 4, according to the two photon excitation selection rules ($\Delta L = 0, 2$, $\Delta J = 0, 2$). Whereas, a two-step excitation is more advantageous because it is possible to select a particular intermediate level with the first laser and then approach the upper levels with the second laser. It is like two separate dipole allowed transitions and one can, in principal, observe certain series through one

level that are forbidden through the other intermediate levels. By this technique, it is possible to provide an unambiguous assignment of the J-value for the excited levels.

The optogalvanic spectra of argon excited from the $3p^5(^2P_{1/2})4p$ $[1/2]_1$, $[3/2]_1$ and $[3/2]_2$ intermediate levels covering the energy region 126575 – 126800 are shown in Fig.7abc.

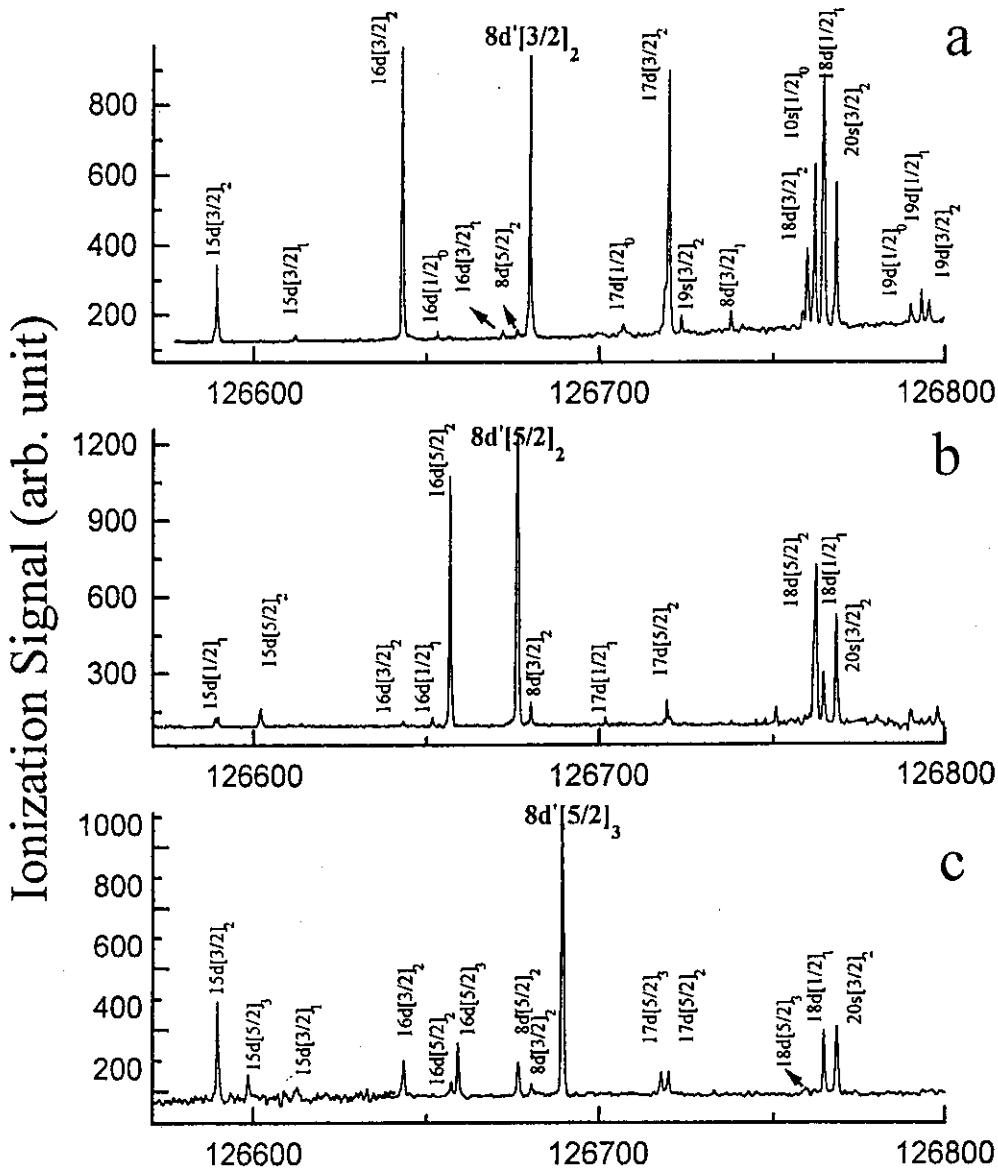

Fig 7: Spectra of argon excited from three intermediate levels.

This region is particularly selected because the $3p^5(^2P_{1/2})8d[3/2]_2$, $3p^5(^2P_{1/2})8d[5/2]_2$ and $3p^5(^2P_{1/2})8d[5/2]_3$ perturbers lie in this region revealing interesting intensity fluctuations. In order to understand the apparent structure, it is important to consider an appropriate coupling scheme for the level designations. The excited levels are therefore designated in

the jℓK-coupling scheme (Racah 1942, Cowan 1981) in which the j of the core electrons weakly coupled with the orbital angular momentum of the excited electron to yield the K-quantum number. K is then coupled with the spin of the excited electron to get the resultant J quantum number and the levels are designated as $j[K]_J$. In the present experiment we have been able to excite three different Rydberg series of definite K and J values from each of the three intermediate levels and the corresponding inter-channel interactions have been studied below and above the first ionization threshold. The selection rules for electric dipole transitions in the jℓK-coupling scheme are: $\Delta\ell = \pm 1$; $\Delta j = 0$; $\Delta K = 0, \pm 1$ and $\Delta J = 0, \pm 1$. It is worth mentioning that these selection rules are well behaved and wherever $\Delta K = \Delta J = +\Delta\ell$, the transition possesses higher intensity. However, the selection rule $\Delta j = 0$ is not followed strictly since transitions with the change of the ionic core are also observed. Consequently the Rydberg series built on the $3p^5(^2P_{3/2})$ and $3p^5(^2P_{1/2})$ ionic levels have been observed with reasonable intensities. The following relatively stronger Rydberg series have been detected from each of the intermediate level converging to the $3p^5(^2P_{3/2})$ and $3p^5\ (^2P_{1/2})$ limits:

(a) $3p^5(^2P_{1/2})4p[1/2]_1 \rightarrow 3p^5(^2P_{3/2})\,nd\ [3/2]_2$
$(^2P_{1/2})\,nd\ [3/2]_2$

(b) $3p^5(^2P_{1/2})4p[3/2]_1 \rightarrow 3p^5(^2P_{3/2})\,nd\ [5/2]_2$
$(^2P_{1/2})\,nd\ [5/2]_2$

(c) $3p^5(^2P_{1/2})4p[3/2]_2 \rightarrow 3p^5(^2P_{3/2})\,nd\ [5/2]_3$
$(^2P_{1/2})\,nd\ [5/2]_3$

The other series such as $3p^5(^2P_{3/2,1/2})ns$ have also been observed but with very weak intensity. In Fig.7a the dominating line is $3p^5(^2P_{1/2})8d\ [3/2]_2$ along with the $3p^5(^2P_{3/2})nd\ [3/2]_2$ series. The $3p^5(^2P_{3/2})16d\ [3/2]_2$ and $3p^5(^2P_{3/2})17d\ [3/2]_2$ also appear with a comparable intensity. In Fig.7b the strongest line is $3p^5(^2P_{1/2})8d\ [5/2]_2$ and the nearby line $3p^5(^2P_{3/2})16d\ [5/2]_2$ is also very prominent. The other members of the $3p^5(^2P_{3/2})nd\ [3/2]_2$ series are very weak. In Fig.7c the $3p^5(^2P_{1/2})8d\ [5/2]_3$ line stands out clearly. The dominating nature of these lines clearly support their identifications as perturbers in the light of the selection rules. In particular, the relative intensities of the three perturbing

levels alter as their excitation paths are changed by selecting different intermediate levels. In Fig.7a, in addition to the $3p^5(^2P_{1/2})8d\ [3/2]_2$ line ($\Delta K = \Delta J = +\ell$) the $3p^5(^2P_{1/2})8d\ [5/2]_2$ line also appears but with very small intensity. The weak nature of this line is in accord with the ΔK selection rule ($\Delta K = 2$ and $\Delta J = +\ell$). In Fig. 7b, the strongest line $3p^5(^2P_{1/2})8d\ [5/2]_2$ obey ($\Delta K = \Delta J = +\ell$) and the weak line$3p^5(^2P_{1/2})8d\ [3/2]_2$ ($\Delta K = 0$ and $\Delta J = +1$). However, all the three perturbers are visible in Fig.7c. The strongest line is $3p^5(^2P_{1/2})8d\ [5/2]_3$ ($\Delta K = \Delta J = +\ell$), the $3p^5(^2P_{1/2})8d\ [5/2]_2$ line is almost ten times weaker as compared to the strong line follows ($\Delta K = 1$ and $\Delta J = 0$) and the weakest line is $3p^5(^2P_{1/2})8d\ [3/2]_2$ according to ($\Delta K = 0$ and $\Delta J = 0$).

The lower members of the series built on the $3p^5(^2P_{1/2})$ level play an interesting role: below the first ionization threshold they interact with the series possessing same K and J values resulting in series perturbations and above the first ionization threshold they decay into the $3p^5(^2P_{3/2})\varepsilon\ell$ adjacent continua and show Fano-type autoionizing line shapes (Fano 1961). Even more interesting fact is that since only one series and the corresponding perturber can be observed from each of the intermediate levels, therefore, one can employ a two-channel model to extract the MQDT parameters below and above the first ionization threshold.

Following the formulation of the multichannel quantum defect theory (Guisti-Suzor and Fano 1984, Cooke and Cromer 1985, Baig and Bhatti, 1994) it is represented in the matrix form as:

$$\begin{vmatrix} \tan\pi(\nu_1+\delta_1) & R_{12} \\ R_{12} & \tan\pi(\nu_2+\delta_2) \end{vmatrix} = 0 \qquad (5)$$

Here δ_1 and δ_2 are the points of maximum contribution of dissociation channels 1 and 2. The ν_1 and ν_2 are the effective quantum numbers related to the term energy of each level according to the Rydberg relation

$$E_n = I_i - \frac{Ry}{(n-\mu_i)} = I_i - \frac{Ry}{\nu_i^2}, \qquad i = 1 \text{ and } 2. \qquad (6)$$

The channel-1 is the series (along with its continuum) terminating to the first ionization limit and channel-2 is the series attached to the second ionization limit, E_n is the term energy, Ry is the mass corrected Rydberg constant for argon 109735.808 cm^{-1} and I_i are the ionization limits $3p^5(^2P_{3/2})$ at 127109.80 cm^{-1} and $3p^5(^2P_{1/2})$ at 128541.38 cm^{-1} respectively (Minnhagen, 1973).

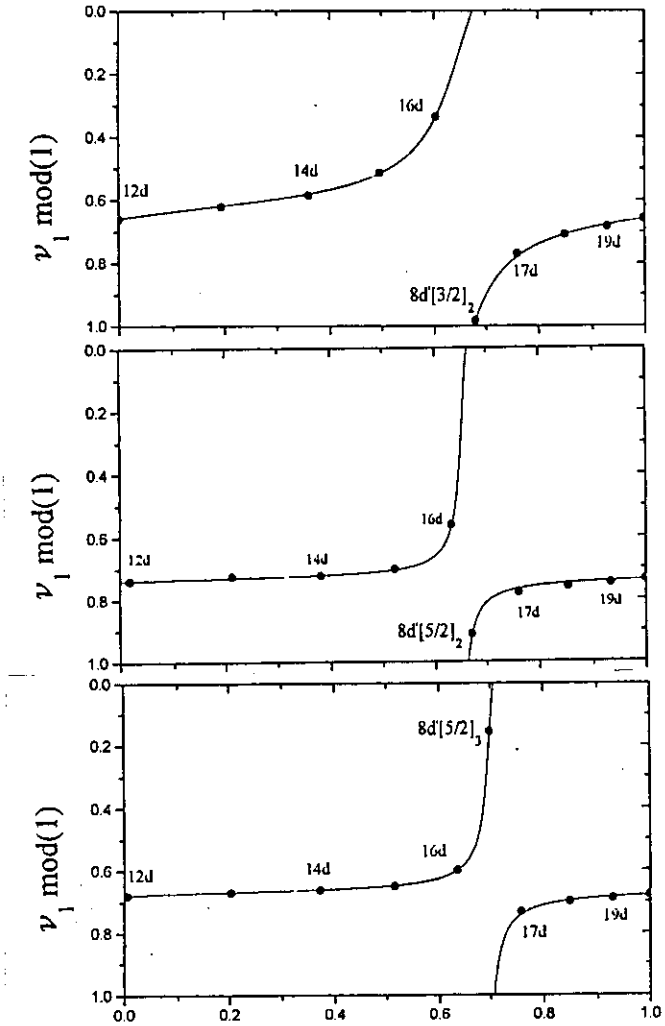

Fig. 8. *The quantum defect plots of the individual series interacting with the intruder of same K and J quantum numbers.*

By plotting the fractional parts of the effective quantum numbers with respect to the second ionization limit on the X-axis and the corresponding mod of the effective quantum number with respect to the first ionization limit on the Y-axis, one can generate the quantum defect plot (Lu and Fano, 1970, Knight, 1986). The analytical relations to determine the allowed energy levels are derived from Eq. (1) and (2) respectively:

$$\nu_1 = \frac{1}{\pi}\tan^{-1}\left(\frac{R_{12}^2}{\tan\pi(\nu_2+\delta_2)}\right) - \delta_1 \qquad (7)$$

and

$$\nu_1 = \nu_2\left(1-\nu_2^2\left[\frac{I_2 - I_1}{Ry}\right]\right)^{-1/2} \qquad (8)$$

The initial values of the parameters δ_1 and δ_2 are readable from the plot i.e., lines parallel to the X-axis give the value of (1 - δ_2) and the line parallel to the y-axis yields the value of (1 - δ_1). The parameter R_{12} is determined by requiring the plot to pass through the experimental data points. More accurate parameters can then be determined using a least squares fitting subroutine.

Fig.8(a,b,c) shows the quantum defect plots for the three series, $3p^5(^2P_{3/2})nd\ [3/2]_2$ series interacting with the $3p^5(^2P_{1/2})8d\ [3/2]_2$ level, $3p^5(^2P_{3/2})nd\ [5/2]_2$ series interacting with the $3p^5(^2P_{1/2})8d\ [5/2]_2$ level and $3p^5(^2P_{3/2})nd\ [5/2]_3$ series interacting with the $3p^5(^2P_{3/2})8d\ [5/2]_3$ level. Since it is a localized perturbation, therefore, we have selected the region in which the effective quantum number with respect to the second ionization limit completes one cycle i.e. υ_2 varies from 7.00 to 8.00. The circles in these figures are the experimental points and the solid curve, which passes through all the data points, represents the Eq. (3). The large avoided crossings between the horizontal and the vertical branches indicate that the $3p^5(^2P_{3/2})nd$ channels are strongly coupled with the $3p^5(^2P_{1/2})nd$ channels. The corresponding MQDT parameters are collected in the Table 1. By inspecting the MQDT parameters, it is clear that the $3p^5nd[3/2]_2$ series shows much stronger interaction, the interaction parameter R_{12} = 0.435, whereas the values for the $3p^5nd[5/2]_2$ and $3p^5nd[5/2]_3$ series are 0.195 and 0.210 respectively. This interaction is further reflected in the autoionization region as the strength of the interaction parameter causes broad autoionizing resonances. Since R_{12} for the $3p^5nd[5/2]_3$ channels is nearly 50% less than that between the $3p^5nd[5/2]_2$ channels, we expect the width of the corresponding autoionizing resonances be of the same ratio and indeed is the case as will be discussed in the next section on the autoionization region.

The calculation of admixture coefficients provide information on the channel mixing and allowing to determine the assignment for each level. The mixing of the channel-2 into the channel-1 is calculated from the relation:

$$\left|A_2^2\right| = \frac{R_{12}^2\{1+\tan^2\pi(\nu_2+\delta_2)\}}{R_{12}^4+\tan^2\pi(\nu_2+\delta_2)+R_{12}^2\{1+\tan^2\pi(\nu_2+\delta_2)\}} \qquad (9)$$

and

$$A_1^2 + A_2^2 = 1$$

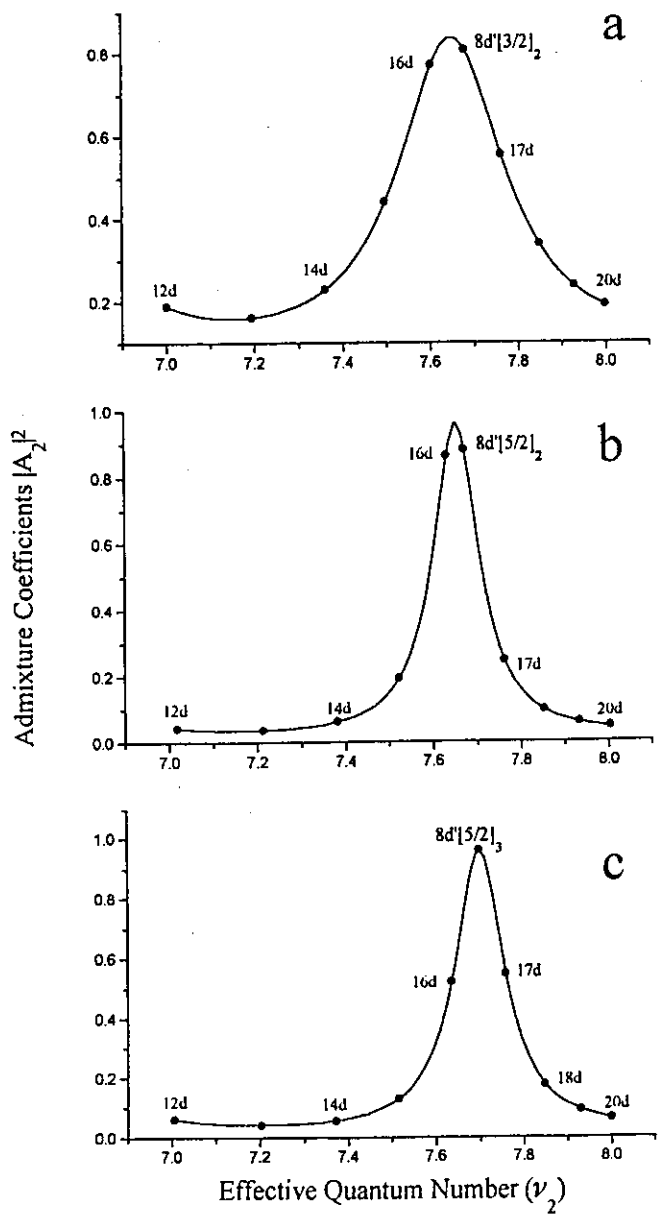

Fig. 9. *The admixture of channel 2 in the channel 1 at different n-values for the individual series*

The admixtures have been determined for the three cases using the equation 5 that are listed in the Table along with the observed and calculated term energies of the levels. It is interesting to examine the composition mixings in the vicinity of the avoided crossings.

The admixing coefficients for all the three Rydberg series are plotted in Fig. 9(a,b,c) that demonstrates the influence of the strength of the interaction parameters. In particular, the $3p^5nd[3/2]_2$ is heavily mixed with the $3p^58d[3/2]_2$ perturber. The mixing is already noticeable 44% and 77% at n = 15 and 16 respectively. The $3p^58d[3/2]_2$ level retains its character with nearly 81% purity and its composition declines to 56%, 34% and 24% at n = 17, 18 and 19 respectively. In the case of $4p^5nd[5/2]_2$ series, the situation is different. The mixing of the $3p^58d[5/2]_2$ perturber is about 19% and 25% for 15d and 17d but the 16d contains very large part nearly 86% of the perturber whereas the $4p^58d[5/2]_2$ level itself is only 88% pure. In the case of $4p^5nd[5/2]_3$ series the mixing of the perturber $4p^58d[5/2]_3$ is about 52% and 55% for 16d and 17d levels whereas the perturber remains 96% pure.

Having done this part of the spectrum, we now look at the autoionizing resonances. As mentioned above, the most probable transitions obey the jℓk-coupling selection rules, consequently, the most prominent series are those that obey the $\Delta K = \Delta J = +\Delta\ell$ selection rules.

The two channel MQDT relation applicable to calculate the photoionization cross section above the first ionization threshold is (Giusti-Suzor and Fano1984), Cooke and Cromer 1985, Ueda 1987, Baig and Bhatti 1994)

$$\sigma = K\frac{[D_1 \tan^2 \pi(\nu_2 + \delta_2) - D_2 R_{12}]^2}{\tan^2 \pi(\nu_2 + \delta_2) + R_{12}^4} \qquad (10)$$

where $K = 4\pi^2 \alpha \hbar \omega$ is a constant that does not change appreciably in the small energy region, D_1 and D_2 are the dipole moments which connect the lower level to the continuum (channel-1) and to the discrete level (channel-2) respectively.

Fig.10a shows the autoionizing resonances $3p^5(^2P_{1/2})9d\ [3/2]_2$ and $3p^5(^2P_{1/2})11s\ [1/2]_{0,1}$ excited from the $3p^5(^2P_{1/2})4p\ [1/2]_1$ intermediate level. The $3p^5(^2P_{1/2})11s\ [1/2]_{0,1}$ resonances have not been included in the simulation as they possess different J-values.

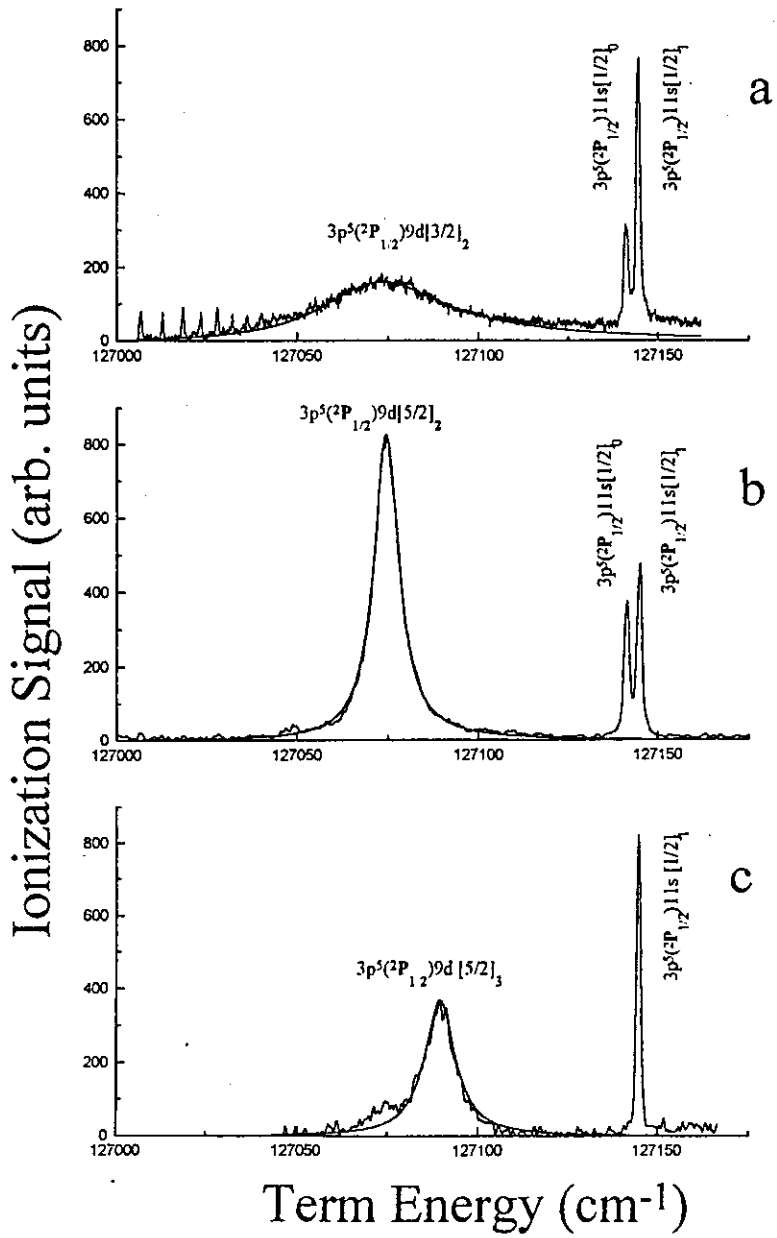

Fig. 10. *The autoionizing resonances adjacent to the first ionization threshold excited from the three different intermediate levels.*

The solid line is the two channel MQDT fit for the $3p^5(^2P_{1/2})9d\ [3/2]_2$ resonance using the parameters R_{12} = 0.435, δ_2 = 0.361, D_1 = -1.5 and D_2 = 5.5. Fig.10b shows the $3p^5(^2P_{1/2})9d\ [5/2]_2$ and $3p^5(^2P_{1/2})11s\ [1/2]_{0,1}$ resonances excited from the $3p^5(^2P_{1/2})4p\ [1/2]_1$ intermediate level. The fitted profile reproduces the strong resonance quite well with the MQDT parameters R_{12} = 0.197, δ_2 = 0.351, D_1 = -0.35 and D_2 = 5.4. The $3p^5(^2P_{1/2})9d\ [5/2]_3$ and $3p^5(^2P_{1/2})11s\ [1/2]_1$ resonances excited from the $3p^5(^2P_{1/2})4p\ [3/2]_2$ intermediate level are reproduced in Fig 10c. The $3p^5(^2P_{1/2})11s\ [1/2]_0$ line is absent here because it is not allowed from the intermediate level. However, the $3p^5(^2P_{1/2})9d\ [3/2]_2$ resonance appear as a shoulder adjacent to the main autoionizing resonance. The solid lines shows the calculated line profiles using the equation 6 and the MQDT parameters: R_{12} = 0.219, δ_2 = 0.306, D_1 = -0.12 and D_2 = 4.2. All these parameters are collected in Table-2.

From the MQDT parameters we can now determine the widths of the autoionizing resonances using the relation

$$\Gamma(cm^{-1}) = \frac{4RyR_{12}^2}{\pi\nu_2^3} \qquad (11)$$

The widths of the three autoionizing resonances $3p^5(^2P_{1/2})9d\ [3/2]_2$, $3p^5(^2P_{1/2})9d\ [5/2]_2$ and $3p^5(^2P_{1/2})9d\ [5/2]_3$ are determined as 41 ± 0.5 cm^{-1}, 8.4 ± 0.5 cm^{-1} and 10.2 ± 0.5 cm^{-1} respectively. However, the widths of these resonances can also be predicted from the quantum defect analysis in the discrete region (see above). Using the parameters listed in Talbe-2, the predicted widths of these resonances are 41 ± 0.5 cm^{-1}, 8.2 ± 0.5 cm^{-1} and 9.4 ± 0.5 cm^{-1} respectively which are remarkably in agreement with the analysis in the autoionizing region. Interestingly these values are also in good agreement with that reduced resonance widths recently reported by Weber et al (1995, 1999).

MQDT Parameters determined in the discrete and the autoionizing regions

Rydberg Series	**Discrete Region**	**Autoionization Region**
(a) $3p^5(^2P_{3/2,1/2})nd[3/2]_2$	R_{12} = 0.435 δ_2 = 0.351 δ_1 = 0.372	R_{12} = 0.435 δ_2 = 0.361 D_1 = -1.5 D_2 = 5.5

(b) $3p^5(^2P_{3/2,1/2})nd[5/2]_2$	R_{12} = 0.195	R_{12} = 0.197
	δ_2 = 0.348	δ_2 = 0.351
	δ_1 = 0.267	D_1 = -0.35
		D_2 = 5.4
(c) $3p^5(^2P_{3/2,1/2})nd[5/2]_3$	R_{12} = 0.210	R_{12} = 0.219
	δ_2 = 0.302	δ_2 = 0.306
	δ_1 = 0.331	D_1 = -0.12
		D_2 = 4.2

Table

(a) Term energies of the $3p^5(^2P_{3/2})$ $nd[3/2]_2$ series and the admixture coefficients in the perturbed region

Assignment	**Term Energy Obs.**	**Term Energy Calc.**	$\|A_1\|^2$	$\|A_2\|^2$
$3p^5$12d$[3/2]_2$	126302.7	126302.4	0.8101	0.1899
13d$[3/2]_2$	126420.9	126420.7	0.8383	0.1617
14d$[3/2]_2$	126515.3	126514.9	0.7707	0.2293
15d$[3/2]_2$	126588.9	126589.0	0.5584	0.4416
16d$[3/2]_2$	126643.1	126643.2	0.2267	0.7733
8d′ $[3/2]_2$	126680.2	126680.2	0.1894	0.8106
17d$[3/2]_2$	126719.6	126719.9	0.4439	0.5561
18d$[3/2]_2$	126759.9	126759.9	0.6604	0.3396
19d$[3/2]_2$	126795.4	126795.2	0.7619	0.2381
20d$[3/2]_2$	126825.8	126825.9	0.8085	0.1915

(b) Term energies of the $3p^5(^2P_{3/2})$ $nd[5/2]_2$ series and the admixture coefficients in the perturbed region

Assignment	**Term Energy Obs.**	**Term Energy Calc.**	$\|A_1\|^2$	$\|A_2\|^2$
$3p^5$12d$[5/2]_2$	126313.4	126313.4	0.9564	0.0436
13d$[5/2]_2$	126432.2	126432.7	0.9620	0.0380
14d$[5/2]_2$	126527.1	126527.0	0.9370	0.0630
15d$[5/2]_2$	126602.1	126602.3	0.8057	0.1943
16d$[5/2]_2$	126656.6	126656.9	0.1357	0.8643
8d′ $[5/2]_2$	126676.4	126676.4	0.1158	0.8842
17d$[5/2]_2$	126719.9	126719.5	0.7532	0.2468
18d$[5/2]_2$	126761.8	126761.5	0.9018	0.0982
19d$[5/2]_2$	126797.6	126797.4	0.9402	0.0598
20d$[5/2]_2$	126828.1	126828.2	0.9545	0.0455

(c) Term energies of the $3p^5(^2P_{3/2})$ nd$[5/2]_3$ series and the admixture coefficients in the perturbed region

Assignment	Term Energy Obs.	Term Energy Calc.	$\|A_1\|^2$	$\|A_2\|^2$
$3p^5$12d$[5/2]_3$	126305.4	126304.7	0.9389	0.0611
13d$[5/2]_3$	126426.2	126425.6	0.9578	0.0422
14d$[5/2]_3$	126521.9	126521.3	0.9431	0.0569
15d$[5/2]_3$	126598.4	126597.8	0.8703	0.1297
16d$[5/2]_3$	126658.8	126658.4	0.4788	0.5212
8d' [5/2]$_3$	126689.4	126689.5	0.0422	0.9578
17d$[5/2]_3$	126717.8	126717.8	0.4526	0.5474
18d$[5/2]_3$	126759.5	126758.9	0.8245	0.1755
19d$[5/2]_3$	126795.6	126795.0	0.9089	0.0911
20d$[5/2]_3$	126826.4	126825.9	0.9373	0.0627

4. Multi-step excitation in lead

Lead possesses two valence electrons in the p-subshell with the ground state as $6p^2\ ^1S_0$. The resonance line 6p7s $(1/2,1/2)_1$ lies in the ultraviolet region. In order to access the high even parity Rydberg sates and the autoionizing resonances, four different intermediate levels are selected pertaining to the 6p7p configuration.

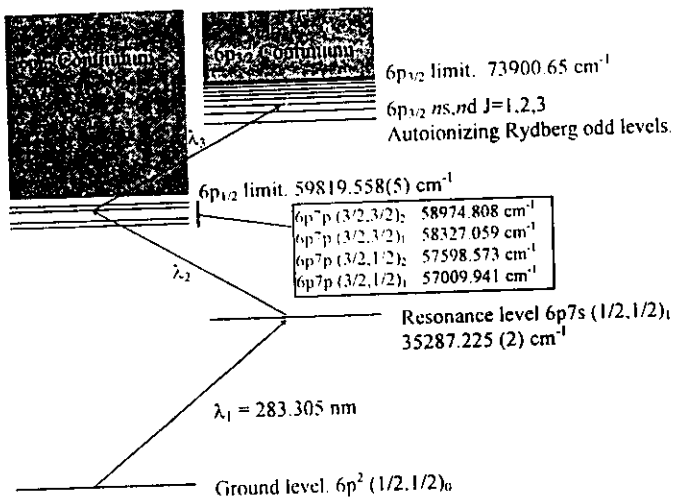

Fig.11 *Excitation scheme for the three-step excitation of the odd-parity autoionizing Rydberg levels of lead.*

The spectra in the energy region from 73180 to 73280 cm^{-1} corresponding to $6p_{3/2}16d$ J = 0, 1, 2, 3 and $6p_{3/2}18s$ J = 1, 2 via the four routes are reproduced in figure 12. It is the lowest multiplet, which could be scanned by the dye lasers for all the four routes. The observation of multiplets from four intermediate levels has enabled us to make the J-value assignments of the upper levels.

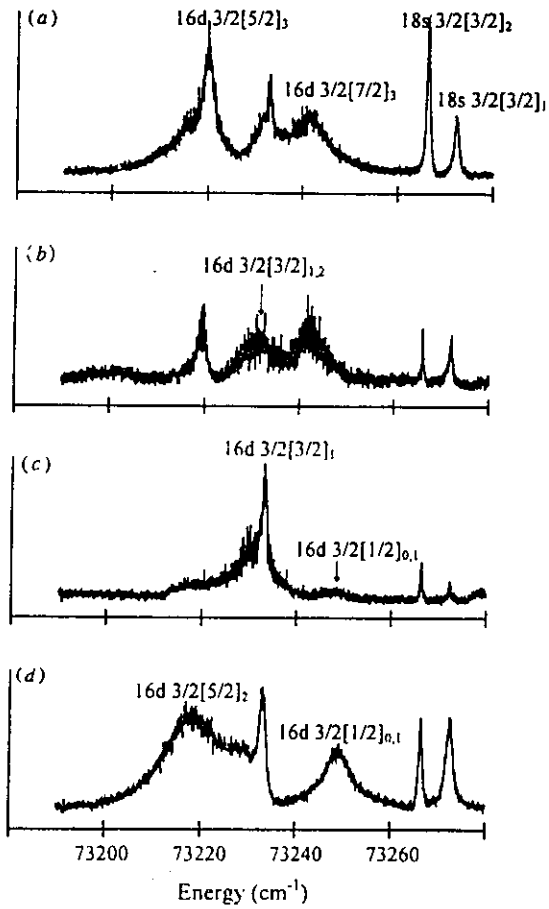

Fig. 12. *The spectra of lead excited from the four 6p3/27p configuration levels to the 6p3/2 nd, ns Rydberg levels. In the j_1K notation the initial levels are (a) $3/2[5/2]_2$, (b) $3/2[3/2]_2$, (c) $3/2[3/2]_1$ and (d) $3/2[1/2]_1$.*

The initial levels belong to the $6p_{3/2}7p$ configuration and, therefore, in the dipole approximation the final state can be either $6pns$ or $6pnd$. For the heavy atoms like lead, in particular for the highly excited levels, j_1K or jj are the appropriate coupling schemes (Cowan and Andrew 1965). In the jj coupling scheme, the selection rules are $\Delta j_1 = 0$, $\Delta j_2 = 0, \pm 1$ and $\Delta J = 0, \pm 1$. From each of the initial $6p_{3/2}7p$ J = 1, 2 levels, the $6p_{3/2}ns$ J = 1,2 will form a doublet. The levels with effective quantum number n^* mod 1 $\approx$ 0.215 were observed by Brown et al (1977), therefore, these levels are assigned as $6p_{3/2}ns$ J = 1. It may be mentioned here that Wood et al (1968) have assigned a low lying level at 49439.6165 cm^{-1}, having effective quantum number $n^* \approx 2.118$ with respect to the $6p_{3/2}$ limit, as 6p7s $(3/2,1/2)_1$. The other nearby levels in the doublet with n^* mod 1 $\approx$ 0.153 are assigned $6p_{3/2}ns$ J = 2. The $6p_{3/2}ns$ doublets appear in all the four spectra as expected.

The $6p_{3/2}nd$ excited levels will form, in the jj coupling scheme, two well separated multiplets $p_{3/2}\ nd(3/2,3/2)_{0,1,2,3}$ and $6p_{3/2}\ nd(3/2,5/2)_{1,2,3,4}$ of three components of individual allowed J values. The component with J = 4 cannot be excited from any of the initial levels. A component with J = 3 will be excited only from an initial level with J = 2 and will be absent in the spectra with J = 1initial level. Similarly, the component of J = 0 will be excited from the J = 1 initial level and will not be observed from the J = 2 initial level. There are three distinct features corresponding to the $6p_{3/2}nd$ excited levels and a well separated doublet corresponding to the $6p_{3/2}ns$ levels in the data shown in Fig 11. Therefore, the jj coupling scheme is not the best description for these levels. The alternative choice would be to designate these levels in the j_1K coupling scheme where j_1 is same as in the jj coupling while the K quantum number is the sum of j_1 and the orbital angular momentum of the excited electron. The total angular momentum J is the vector addition of K and the spin of the excited electron. The selection rules for this scheme are $\Delta j_1 = 0$, $\Delta K = 0, \pm 1$ and $\Delta J = 0, \pm 1$. The initial 6p7p$(3/2,1/2)_2$ level in the j_1K coupling scheme is represented by 6p7p $3/2[5/2]_2$ with $j_1[K]_J$ notation (Cowan and Andrew 1965). From this level the $6p_{3/2}ns$ excited levels will form a doublet $6p_{3/2}ns$ $3/2[3/2]_{1,2}$ as in the jj coupling. However, the allowed $6p_{3/2}nd$ excited levels will be $6p_{3/2}nd$ $6p_{3/2}nd$ $3/2[3/2]_{1,2}$, $3/2[5/2]_{2,3}$ and $3/2[7/2]_3$. i.e. There will be three well resolved features corresponding to

the individual K values, whereas, features corresponding to the K= 3/2, 5/2 will be comprising of doublet components for individual J values. Indeed, there are three distinct features in the observed spectrum (see Fig.12a). Similarly, From the 6p7p(3/2,3/2)$_2$ level which corresponds to 6p7p 3/2[3/2]$_2$ in the j_1K scheme, the allowed 6p$_{3/2}$*n*d excited levels will be 3/2[1/2]$_1$, 3/2[3/2]$_{1,2}$, 3/2[5/2]$_{2,3}$. Again there are three expected features and indeed three features are observed (see Fig.12b). The middle feature of the spectra in Fig.12b is broad while, in Fig.12a, there is a relatively sharp peak on the higher energy side. This peak has n* mod 1 $\approx$ 0.82. The levels with identical n^* are reported by Brown et al (1977) and, therefore, it must have J = 1. Therefore, the sharp features are assigned 6p$_{3/2}$16d 3/2[3/2]$_1$. In the work of Brown et al (1977) these levels do not appear as absorption lines but as deep window resonances, whereas, in the present work they appear as strong symmetric absorption lines. It is understandable, since in this experiment the initial levels are mostly of 6p$_{3/2}$7p configuration and, therefore, the transitions to the 6p$_{3/2}$*n*d levels possess a very high value for the Fano's q parameter. However, in the work of Brown et al (1977) the initial level is the ground level, which has a very little contribution of the 6p$_{3/2}$6p$_{1/2}$ configuration resulting in a highly asymmetric Fano profiles. The other component, 6p$_{3/2}$*n*d 3/2[3/2]$_2$ is not resolvable. In Fig.12b it has comparable intensity to that of the J = 1 component, while in Fig.12a,c,d its intensity is reduced and it appears as a lower energy side shoulder.

The assignment of the first feature on the lower energy side is straight forward. Wood et al (1965) observed and assigned the 6p6d 3/2[5/2]$_2$ and 3/2[5/2]$_3$ levels at energies 58517.607 cm^{-1} (n^* = 2.671) and 59186.62 cm^{-1} (n^* = 2.73) respectively. The higher J value component lies on the higher side. Therefore, the sharp peak on the higher energy side of the feature with n* mod 1 $\approx$ 0.79 would have the assignment 3/2[5/2]$_3$. The J = 2 component appears as shoulder on the lower energy side. In figures 12c and 12d, the J = 3 component should not and does not appear because of the strict ΔJ selection rule. However, the J = 2 component appears very strongly in Fig.12d although it is equally weak in Fig.12c.

The two features discussed above have same assignments for the two spectra Fig.12a and Fig.12b. The third feature in the Fig.12a is expected to be $6p_{3/2}nd$ $3/2[7/2]_3$ while in Fig.12b it is $6p_{3/2}nd$ $3/2[1/2]_1$. However, they appear at the same energy in both the spectra with n^* mod 1 $\approx$ 0.90, and so they cannot be different. This puzzle is resolved when the spectrum in Fig.12c is examined. Here the initial level is $6p7p(3/2,3/2)_1$ or 6p7p $3/2[3/2]_1$ in jj and j_1K coupling schemes respectively. Therefore, the allowed final $6p_{3/2}16d$ levels are $6p_{3/2}16d$ $3/2[1/2]_{0,1}$, $3/2[3/2]_{1,2}$ and $3/2[5/2]_2$. The later of these levels appears as a weak shoulder in the Fig.12a and Fig.12b and does not convincingly show up here in Fig.12c either. The $3/2[3/2]_{1,2}$ feature is common in all the spectra. Now the third feature appearing in Fig.12a and Fig.12b does not show up here in Fig.12c. Instead, a weak feature appears on the higher energy side with n^* mod 1 $\approx$ 0.97. Similarly, the third feature of the Fig.12a,b is missing in Fig.12d while a strong feature with n^* mod 1 $\approx$ 0.98 is present. At these values of n^* Brown et al (1977) also observed a series. Putting these together, the levels with n^* mod 1 $\approx$ 0.97 and 0.98 are assigned as $6p_{3/2}nd$ $3/2[1/2]_{0,1}$. The J = 0 component is not expected in the Fig.12a and Fig.12b spectra owing to the ΔJ selection rule. The J=1 component is also not expected in Fig.12a because it will be very weak since $\Delta K = 2$ is in violation of the ΔK selection rule. However, J = 1 component is allowed in Fig.12b but $3/2[1/2]_{0,1}$ is located at a position such that it gets buried underneath the shoulder of the third feature. Therefore, the third feature in Fig.12a and Fig.12b with n^* mod 1 $\approx$ 0.90 may be assigned as $3/2[7/2]_3$. Its appearance in the Fig.12b is attributed to the weakness of the ΔK selection rule. The $3/2[1/2]_0$ appear distinctly in Fig.12c and $3/2[1/2]_1$ quite strongly in Fig.12d. In Fig.12d, a strong and broad feature near the position of $3/2[5/2]_3$ emerges. This has been assigned $3/2[5/2]_2$ since J = 3 is not allowed in this spectrum. This feature which is allowed in all the four spectra, shows up weakly as lower energy shoulder in Fig. 12a,b and a little bump in Fig.12c. A large disparity in the widths of the two components of the K = 5/2 feature with J = 2, 3 is intriguing. The comparison of the energies of the two components of the K = 5/2 reveals that energetically they are very close but at the same time their FWHM (full width at half maximum) is enormously different.

References

Baig M A and Bhatti S A 1994 *Phys. Rev. A* **50**, 2750

Baig M A, Yaseen M, Nadeem A, Ali R and Bhatti S A 1998, *Optics Commun.* **156**, 279

Baig M A, Yaseen M, Ali R, Nadeem A and Bhatti S A 1998, *Ochem.Phys.Lett.* **296**, 403

Bhatti S A, Nwaz M, Farooqi S M, Ahad A, Butt S, Ahmad N and Baig M A 1997 *J.Phys.B: Atom Mol Opt Phys.* **30**, 1179

Berkowitz J, "Photoabsorption, Photoionization and Photoelectron Spectroscopy" Academic Press, New York, 1979.

Brown C M, Tilford S G and Ginter M L, 1977, *J. Opt. Soc. Am,* **67** 1240

Cooke W E and Cromer C L, 1985, *Phys. Rev. A*, **32**, 2725

Connerade JP 1998 "*Highly Excited Atoms*" Cambridge University Press.

Cowan R D, 1981, 'The Theory of Atomic Structure and Spectra', California

Cowan R D and Andrew K L, 1964, *J. Opt. Soc. Am*, **55**, 502

Demtroeder W 1998 "*Laser Spectroscopy*" Springer Verlag, Berlin

Fano U 1961 *Phys.Rev.* **A15** 1920

Fano U, 1975, *J. Opt. Soc. Am*,**65**, 979

Gallagher TF, 1994 "*Rydberg Atoms*" Cambridge University Press.

Hanna D, Karkainen P, Wyatt R, 1975 *Opt. Quan. Elect.* 7, 115

Letokhov VS 1987 "Laser Photoionization Spectroscopy" Academic Press Orlando. FL

Moore C E, 1971, *Atomic Energy Levels I,II, III* (Washington DC: NBS)

Ueda K 1987 Phys. Rev. A **35** 2484

Wood D R and Andrew K L, 1968, *J.Opt.Soc.Am.* **58**, 818